AJNR

Trigeminal Ganglion and its Divisions: Detailed Anatomic MR Imaging with Contrast-Enhanced 3D Constructive Interference in the Steady State Sequences

Indra Yousry, Bernhard Moriggl, Urs D. Schmid, Thomas P. Naidich and Tarek A. Yousry

AJNR Am J Neuroradiol 2005, 26 (5) 1128-1135
http://www.ajnr.org/content/26/5/1128

Trigeminal Ganglion and its Divisions: Detailed Anatomic MR Imaging with Contrast-Enhanced 3D Constructive Interference in the Steady State Sequences

Indra Yousry, Bernhard Moriggl, Urs D. Schmid, Thomas P. Naidich, and Tarek A. Yousry

BACKGROUND AND PURPOSE: **Visualization of the trigeminal system is important for imaging diagnosis but technically challenging. We assessed how well the trigeminal ganglion, its rootlets, and its branches (V1, V2, and V3) are depicted on three high-resolution pulse sequences.**

METHODS: **Twenty-two patients (44 sides) underwent nonenhanced 3D constructive interference in the steady state (CISS) MR imaging. Two of these patients and another 20 (44 sides) also underwent contrast-enhanced 3D CISS and contrast-enhanced 3D time-of-flight (TOF) MR angiographic (MRA) imaging. Appearances of the ganglion, sinus ganglii, ganglion lip, and sensory and motor rootlets in the Meckel cave were assessed.**

RESULTS: **The trigeminal ganglion was shown on enhanced 3D CISS images in all cases, on nonenhanced 3D CISS images in 77.3%, and on enhanced 3D TOF MRA images in 92.9%. Sinus ganglia and lips were demonstrated on 98% of enhanced 3D CISS images. Sensory rootlets were depicted with all 3D CISS sequences but no 3D TOF sequences. V1, V2, and V3 were displayed with all enhanced 3D TOF MRA sequences, 79.5–100% of enhanced 3D CISS sequences, and 0–50% of nonenhanced 3D CISS sequences.**

CONCLUSION: **The enhanced 3D CISS sequence was best for displaying the trigeminal ganglion, sinus ganglii, and sinus lips, whereas the enhanced 3D TOF sequence best displayed the emerging V1, V2, and V3 roots. The enhanced 3D CISS sequence was most useful. Complete MR imaging evaluation of the trigeminal ganglion and roots is best performed by using enhanced 3D CISS and enhanced 3D TOF MRA sequences.**

The trigeminal (semilunar or gasserian) ganglion is situated along the anterior inferior lateral wall of the Meckel cave (1–4) (Fig 1). The ganglion presents a convex surface that merges with the anteroinferolateral dural wall of the sinus and a concave posteromedial surface (designated the sinus ganglii) that faces CSF in the Meckel cave (the trigeminal cistern) (3, 5, 6). The margins of the concave sinus ganglii are designated the ganglion lips (5, 6). Three major divisions (V1, V2, and V3) of the trigeminal nerve (cranial nerve [CN] V) arise from the convex face of the ganglion (1–4) (Fig 1). A group of small sensory rootlets, collectively designated the pars triangularis (5), emerge from the concave sinus ganglii to form the sensory root of CN V (2, 5, 7). The motor root of CN V courses along the medial aspect of the sensory fibers (8) and then passes inferior to the ganglion (9).

Previous authors have used contrast-enhanced T1-weighted MR imaging to evaluate the trigeminal ganglion (10) and nonenhanced 3D constructive interference in the steady state (3D CISS) MR images to evaluate the anatomy of the sensory and motor roots of the trigeminal nerve in the Meckel cave (11, 12). However, T1-weighted images do not display the fine detail of the ganglion and rootlets, while nonenhanced 3D CISS images inadequately display the trigeminal ganglion (13, 14). These findings suggested that contrast-enhanced 3D CISS sequences might depict the microanatomy of both the ganglion and the roots well. In the region of the Meckel cave, planning

Received April 28, 2004; accepted after revision September 17.

From the Department of Neuroradiology, Klinikum Grosshadern, Ludwig-Maximilians University, Munich, Germany (I.Y.); the Institute of Anatomy, Histology, and Embryology, Medical University Innsbruck, Austria (B.M.); the Neurosurgical Unit, Klinik Im Park, Zurich, Switzerland (U.D.S.); the Department of Radiology, Section of Neuroradiology, Mount Sinai Medical Center, New York, NY (T.P.N.); and the Lysholm Department of Neuroradiology, Institute of Neurology, London, UK (T.P.N., T.A.Y.).

Address correspondence to Dr. med. Indra Yousry, Department of Neuroradiology, Klinikum Grosshadern, Marchioninistr. 15, D-81377 Munich, Germany.

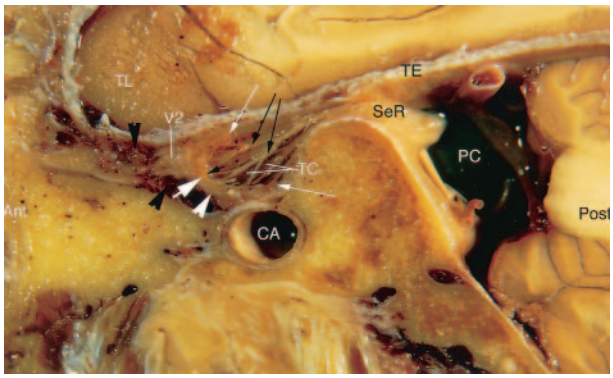

FIG 1. Sagittal cryomicrotomic section through the Meckel cave in the plane of the trigeminal nerves was obtained from the right medial aspect of a cadaveric specimen from a 74-year-old woman. Small portion of the sensory root (*SeR*) is seen at its entry into the cave. Trigeminal ganglion (*thick white arrow*) is at the anterior aspect of the cave, and anterior margin of the ganglion adheres to the dural wall (*white arrowhead*). Multiple sensory rootlets (*long black arrows*) arise from the concave medial surface of the ganglion (sinus ganglii) (*short black arrow*) to course in the trigeminal cistern (*TC*). Superior and inferior lips of the ganglion (*thin white arrows*) are particularly well displayed. Portion of the maxillary nerve (*V2*) shown in this plane is surrounded by venous channels (*black arrowheads*) along the inferior border of the cavernous sinus. *Ant* = anterior, *CA* = carotid artery, *PC* = prepontine cistern, *Post* = posterior, *TE* = cerebellar tentorium, *TL* = temporal lobe.

for successful microsurgery requires both knowledge of the typical gross anatomy in cadavers (2, 8, 15, 16) and knowledge of the specific anatomy and variations in the individual patient *in vivo*. Therefore, the aim of this microanatomic study was to determine how well contrast-enhanced 3D CISS sequences demonstrate the trigeminal ganglion; display the fine anatomy of the ganglion, sinus ganglii, sinus lips, and sensory and motor rootlets; and depict the cranial and/or foraminal segments of V1, V2, and V3 in comparison with the T1-weighted and nonenhanced 3D CISS sequences previously reported.

Methods

Patients

The study group included 42 patients (21 men, 21 women; age range, 20–74 years; mean age, 52.5 years) who were to undergo MR study for a reason unrelated to our purpose (e.g., evaluation of supratentorial parenchymal hemorrhage, infarction, or tumor that did not affect the infratentorial compartment). The patients agreed to undergo imaging with extra (enhanced) 3D CISS and 3D time-of-flight (TOF) MR angiographic (MRA) sequences. None of the patients had known clinical abnormalities affecting CN V or any other pathology affecting the infratentorial region. The review board of our department approved our study, which conformed to the Helsinki declaration. All patients gave their informed consent.

MR Imaging Procedures

All imaging was performed by using a 1.5-T system (Magnetom Vision; Siemens, Erlangen, Germany) with the regular quadrature head coil. Two pulse sequences were used: (1) a 3D CISS sequence with TR/TE/NEX = 12.25/5.90/1, flip angle = 70° field of view (FOV) = 180 × 180 mm (read × phase encode), slab thickness = 70.0 mm, matrix = 512 × 262, number of 3D partitions = 106, number of slabs = 1, pixel size = 0.35 × 0.69 mm, effective section thickness = 0.66 mm, and imaging time = 11.4 minutes, and (2) a 3D TOF sequence performed before and 3 minutes after the administration of gadopentate dimeglumine 0.1 mmol/kg, with TR/TE/NEX = 31/7/1, flip angle = 20°, FOV = 200 mm, slab thickness = 50 mm, matrix = 512 × 224, number of 3D partitions = 50, number of slabs = 1, pixel size = 0.78 × 0.39, effective section thickness = 1 mm, and imaging time = 5 minutes 49 seconds.

Twenty-two patients (44 sides) underwent nonenhanced 3D CISS MR imaging. In two of these patients and in an additional 20 (44 sides), contrast-enhanced 3D CISS and contrast-enhanced 3D TOF MRA sequences were performed 3 minutes after the intravenous administration of gadopentate dimeglumine 0.1 mmol/kg. The 42 patients who underwent contrast-enhanced imaging always received the contrast-enhanced 3D TOF sequence first followed by the contrast-enhanced 3D CISS sequence.

Image Analysis

The data sets from each 3D CISS and 3D TOF sequence were reconstructed in three orthogonal oblique planes oriented in relation to the cisternal course of the sensory root of CN V. These planes were designated transverse, coronal, and sagittal. Transverse signified the horizontal plane that was parallel to the course of the cisternal course of the sensory root of CN V, whereas coronal signified the coronal plane perpendicular to the cisternal course of the sensory root of CN V. All images were analyzed by two experienced neuroradiologists (I.Y., T.A.Y.) who had completed their training and who had 9 and 20 years of experience in neuroradiology and radiology, respectively. Images were analyzed and scored collaboratively.

Anatomic Assessment of the Trigeminal Ganglion

The certainty of identifying the trigeminal ganglion was determined for each pulse sequence in each of the transverse, sagittal and coronal planes and recorded on an arbitrary scale, where a score of 2 was identified with certainty, 1 was most probable identification, and 0 was not identified (17–20). The trigeminal ganglion has an anatomically well-known semilunar form (5, 6, 8, 15) and location (at the anterior, inferior, and lateral aspects of the Meckel cave) (6, 8, 10, 15, 21). Clear recognition of this typical structure was considered positive identification. If this structure was not visible, negative identification was recorded.

In all cases with contrast enhancement, the intensity of enhancement in the trigeminal ganglion was visually determined on 3D TOF MRA and 3D CISS images. The ganglion was identified with certainty when the enhancing ganglion was clearly distinguishable from the less prominently enhancing dura (corresponding to strong ganglial enhancement). Most probable identification was when the ganglion enhanced only slightly more than the moderate enhancement of the dura. Mild enhancement was when the ganglion could not be identified because of the lack of differential enhancement between the ganglion and the dura.

The certainty of identifying the sinus ganglii and the lower and upper lips of the ganglion was determined in the sagittal plane. The typical semilunar form of the trigeminal ganglion consisted of the convex anterior surface and the concave posterior surface (the sinus ganglii). The lips of the ganglion were anatomically defined as the rim of the concave surface of the ganglion (5, 6, 22). Recognition of this anatomically well-known concave surface and of the upper and lower margins of this surface was considered positive identification.

The thickness of the ganglion was determined as the greatest anteroposterior dimension of the ganglion measured in the sagittal plane with each of the three sequences. Measurements were performed directly on the evaluation console of the MR

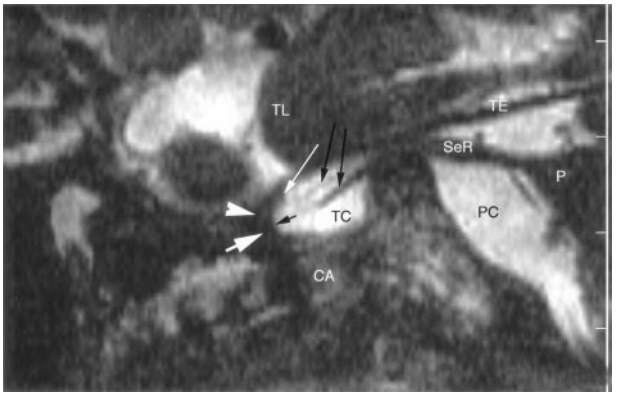

FIG 2. Sagittal nonenhanced 3D CISS image through the right side of the Meckel cave in a 58-year-old woman. Sensory root (*SeR*) is shown from its apparent origin at the pons (*P*) to the entrance of the cave. Ganglion (*thick white arrow*) at the anterior aspect of the cave is difficult to identify, and anterior margin of the trigeminal ganglion cannot be distinguished from the dural wall (*arrowhead*) of the cave. Only the superior lip of the ganglion (*thin white arrow*) is well defined. One smaller and one larger sensory rootlet (*long black arrows*) arise from the sinus ganglii (*short black arrow*) and course in the trigeminal cistern (*TC*). Maxillary nerve is not depicted at the inferior border of the cavernous sinus. *CA* = carotid artery, *PC* = prepontine cistern, *TE* = cerebellar tentorium, *TL* = temporal lobe.

unit. Measurements were simplified by using a multiplanar reconstruction (MPR) software program supplied by the manufacturer (Siemens) that allowed us to measure distances in any desired plane. Using this program, we selected the sagittal plane through the center of the ganglion. The distance was then determined from the most anterior point of the convex surface (apex of the anterior circumference) of the ganglion up to the sinus ganglii. The distance was determined from the most anterior point of the convex surface to the concave inside of the ganglion. The thickness could be determined only in those ganglia in which the anterior convex surface could be defined and distinguished from the adjacent dura.

Anatomic Assessment of the Sensory and Motor Rootlets in the Meckel Cave

The certainties of identifying the motor root and the sensory rootlets of the pars triangularis were independently assessed in the sagittal plane and scored as described earlier.

Anatomic Assessment of the Main Trigeminal Branches

The certainties of identifying the cranial and foraminal segments of the ophthalmic nerve (V1), the maxillary nerve (V2), and the mandibular nerve (V3) were independently determined in each of the transverse, sagittal, and coronal planes and recorded by using the same arbitrary scale as described earlier.

Results

Identification and Dimensions of the Trigeminal Ganglion

Overall and for each one of the three orthogonal planes, the contrast-enhanced 3D CISS sequence was superior to the nonenhanced 3D CISS sequence or the contrast-enhanced 3D TOF sequence in depicting the trigeminal ganglion (Figs 2–5) (Table 1). The most useful sequence was the sagittal contrast-enhanced 3D CISS sequence, with which 100% of the ganglia were identified and 79.5% were scored 2. The two contrast-enhanced sequences showed the ganglion better than the nonenhanced 3D CISS sequence. The thickness of the ganglion was determined less often by using the nonenhanced 3D CISS sequence (n = 26, 59.1%) compared with the enhanced 3D CISS (n = 43, 97.8%) and 3D TOF (n = 39, 92.9%) sequences (Table 2). The trigeminal ganglion was usually 2 mm thick; less commonly, 1 mm; and rarely, 3 mm.

Identification of Upper and Lower Ganglion Lips and Sinus Ganglia

Identification of these structures was positive when all three elements were identified: the upper and lower lips of the ganglion and the sinus ganglii. The upper and lower lips of the ganglion and the sinus ganglii were best demonstrated by using the contrast-enhanced 3D CISS sequence (98%) (Figs 3 and 4, Table 3). The contrast-enhanced 3D TOF sequence (78.5%) was slightly superior to the nonenhanced 3D CISS sequence (77.3%) overall (Figs 2 and 5), but the percentage of positive identifications (score of 2) was higher with the nonenhanced 3D CISS sequence than with the 3D TOF sequence.

Identification of Sensory and Motor Rootlets

The sensory fibers emerging from the trigeminal ganglion were identified with certainty (score of 2) on all nonenhanced and the contrast-enhanced 3D CISS images (Figs 2–4). The motor root was depicted with certainty and differentiated from the sensory fibers in all cases on nonenhanced and enhanced 3D CISS images. However, the sensory and motor roots were not identified (score of 0) on any 3D TOF MRA image in any plane (Fig 5).

Identification of the Ophthalmic, Maxillary, and Mandibular Nerves

The course of V1 in the lateral wall of the cavernous sinus and in the superior orbital fissure was best identified with the contrast-enhanced 3D TOF sequence (100% in each imaging plane) (Fig 5, Table 4). V1 was well depicted on contrast-enhanced 3D CISS images (100% in the transverse plane, 91–97.7% in the other planes). Nonenhanced 3D CISS images did not display V1 adequately.

The course of V2 at the inferior border of the cavernous sinus and inside foramen rotundum was identified best by using the contrast-enhanced 3D TOF sequence (100% in the transverse and sagittal planes, 97.6% in the coronal plane) (Fig 5). V2 was well depicted on contrast-enhanced 3D CISS images in 84.1–93.2% (Figs 3 and 4). V2 was not adequately displayed by using the nonenhanced 3D CISS sequence (Fig 2).

The course of V3 in the foramen ovale was best identified by using the contrast-enhanced 3D TOF sequence (100% in each imaging plane), and it was

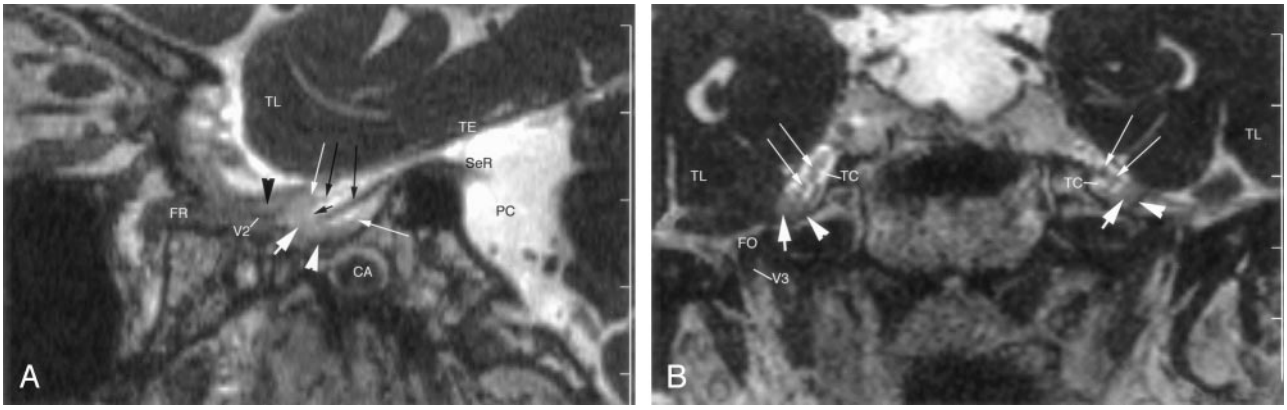

FIG 3. Enhanced 3D CISS images through the right side of the Meckel cave in a 62-year-old woman. TL = temporal lobe.

A, Sagittal image shows a small portion of the sensory root (*SeR*) at its entry into the cave. Trigeminal ganglion (*thick white arrow*) and its lips (*thin white arrows*) are shown at the anterior end of the cave. Anterior margin of the ganglion is clearly differentiated from the dural wall (*white arrowhead*) of the cave. Two sensory rootlets (*long black arrows*) emerge from the sinus ganglii (*short black arrow*) and pass through the trigeminal cistern. Maxillary nerve (*V2*) courses along the inferior wall of the cavernous sinus, surrounded by enhancing venous channels (*black arrowhead*). *CA* = carotid artery, *FR* = foramen rotundum, *PC* = prepontine cistern, *TE* = cerebellar tentorium.

B, Coronal image shows the cave bilaterally. Trigeminal ganglion (*thick white arrows*) lies along the anteroinferior border of the cave. Less-enhancing dura (*arrowheads*) is clearly differentiated from the ganglion. Multiple, small sensory rootlets (*thin white arrows*) are seen in the trigeminal cistern (*TC*). Mandibular nerve (*V3*) is partly shown on the right side in the foramen ovale (*FO*).

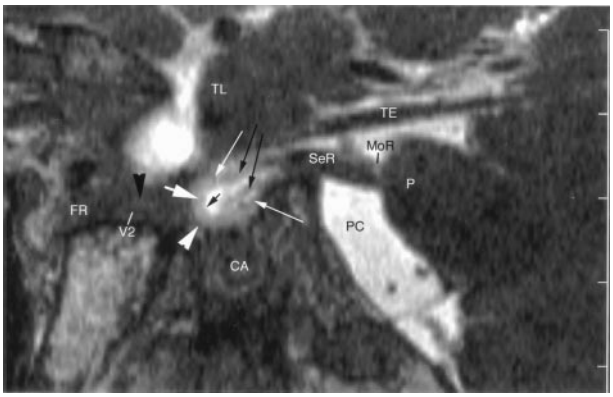

FIG 4. Sagittal enhanced 3D CISS image through the right side of the Meckel cave in a 54-year-old man. Sensory root (SeR) is displayed from its apparent origin at the pons (*P*) to the entrance of the cave. Trigeminal ganglion (*thick white arrow*) is at the anteroinferior border of the cave. Anterior margin of the enhancing ganglion is clearly distinguished from the less-enhancing dura (*white arrowhead*) of the cave. Lips of the ganglion (*thin white arrows*) define the sinus ganglii (*short black arrow*) from which small sensory rootlets (*long black arrows*) arise. Maxillary nerve (*V2*) is depicted along the inferior border of the cavernous sinus, surrounded by venous channels (*black arrowhead*) en route to the foramen rotundum (*FR*). *CA* = carotid artery, *MoR* = motor root of the trigeminal nerve at its point of exit, *PC* = prepontine cistern, *TE* = cerebellar tentorium, *TL* = temporal lobe.

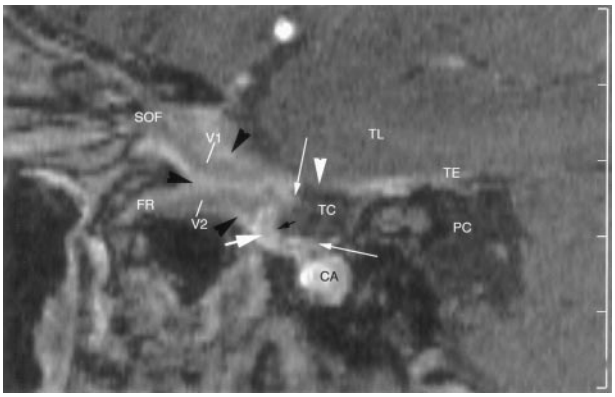

FIG 5. Sagittal enhanced 3D TOF image through the right side of the Meckel cave in a 53-year-old-man. Enhancing ganglion (*thick white arrow*) is shown at the anteroinferior margin of the cave, in continuity with the dural wall (*white arrowhead*). Superior and inferior lips of the ganglion (*thin white arrows*) are well depicted. No sensory rootlets are seen in the trigeminal cistern (*TC*). Ophthalmic nerve (*V1*) and maxillary nerve (*V2*) are hypointense, linear structures surrounded by strongly enhancing venous channels (*black arrowheads*) in the lateral wall and along the inferior border, respectively, of the cavernous sinus. V2 enters the foramen rotundum (*FR*), while V1 passes to the superior orbital fissure (*SOF*). *CA* = carotid artery, *PC* = prepontine cistern, *TE* = cerebellar tentorium, *TL* = temporal lobe.

well depicted by using the contrast-enhanced 3D CISS sequence (100% in the coronal and sagittal planes, 79.5% in the transverse plane) (Fig 3). Nonenhanced 3D CISS images displayed V3 better than V2 or V1, but they were inadequate for consistent identification.

Discussion

The contrast-enhanced 3D CISS sequence depicted the trigeminal ganglion, the sinus ganglii and its lips, the sensory roots in the Meckel cave, and the motor root coursing along the floor of the Meckel cave well. For these structures, the contrast-enhanced 3D CISS sequence was superior to the nonenhanced 3D CISS and the contrast-enhanced 3D TOF sequences. The contrast-enhanced 3D CISS sequence also provided excellent depiction of the three main trigeminal branches (V1, V2, and V3), although the contrast-enhanced 3D TOF sequence was better for displaying these nerves.

Meckel Cave and its Contents

The Meckel cave is an enclosure formed by two layers of dura: an internal layer of dura propria and

TABLE 1: Identification of the trigeminal ganglion

	Plane and Score*								
	Sagittal			Transverse			Coronal		
Study	2	1	0	2	1	0	2	1	0
Nonenhanced 3D CISS (44 sides)	7 (15.9)	27 (61.4)	10 (22.7)	2 (4.5)	19 (43.2)	33 (75)	2 (4.5)	16 (36.4)	26 (59.1)
Enhanced 3D CISS (44 sides)	35 (79.5)	9 (20.5)	0 (0)	32 (72.7)	12 (27.3)	0 (0)	22 (50)	19 (43.2)	3 (6.8)
Enhanced 3D TOF (42 sides)	32 (76.2)	7 (16.7)	3 (7.1)	16 (38.1)	17 (40.5)	9 (21.4)	20 (47.6)	14 (33.3)	8 (19)

Note.—Data are numbers of ganglia (percentage).
*Scores: 2 = positive identification, 1 = highly probable identification, 0 = no identification.

TABLE 2: Thickness of the trigeminal ganglion in the sagittal plane

	Thickness of Ganglion			
Study	Not Determined	1 mm	2 mm	3 mm
Nonenhanced 3D CISS (44 sides)	18 (40.9)	11 (25)	14 (31.8)	1 (2.3)
Enhanced 3D CISS (44 sides)	1 (2.3)	12 (27.3)	31 (70.5)	0 (0)
Enhanced 3D TOF (42 sides)	3 (7.1)	12 (28.6)	27 (64.3)	0 (0)

Note.—Data are numbers of ganglia (percentage).

TABLE 3: MR imaging identification of upper and lower lips of the ganglion and sinus ganglii in the sagittal plane

	Score*		
Study	2	1	0
Nonenhanced 3D CISS (44 sides)	19 (43.2)	15 (34.1)	10 (22.7)
Enhanced 3D CISS (44 sides)	42 (95.5)	1 (2.5)	1 (2.5)
Enhanced 3D TOF (42 sides)	4 (9.5)	29 (69)	8 (19)

Note.—Data are numbers of ganglia (percentage).
*Scores: 2 = positive identification, 1 = highly probable identification, 0 = no identification.

an external layer of intracranial periosteum (3, 6, 22). The subarachnoid space extends upward from the prepontine cistern to form the trigeminal cistern in the cave (3, 5, 6). This cistern extends forward from the porus trigeminus to approximately the level of the midportion of the trigeminal ganglion (8).

The trigeminal ganglion is a thin crescent-shaped (semilunar) structure (5, 6) that lies at the anterior, inferior, and lateral aspects of the Meckel cave (6, 10, 21). The convex surface of the ganglion is directed toward the anteroinferolateral walls of the Meckel cave (5). The concave posteromedial surface, designated the sinus ganglii, is directed posterosuperomedially toward the trigeminal cistern and the ostium of the Meckel cave (9, 22). The margins of the sinus ganglii represent the lips of the ganglion (5, 22). The size of the ganglion varies widely (3, 6), ranging from 14 to 22 mm in length and from 4 to 5 mm in overall thickness (anteroposterior dimension) (5–7). However, after one accounts for its concave shape, the true thickness of the ganglion is 1.5–2 mm (5, 9). An envelope of dura propria and arachnoid encloses the ganglion (2, 3, 5, 6). The posteromedial portion of the ganglion lies in the trigeminal cistern, but the convex anteroinferior surface of the ganglion is extremely adherent to the dura of the Meckel cave in its medial aspect and to the dura of the temporal fossa in its lateral aspect (2, 3, 5, 6, 22). Therefore, this portion lies outside the cistern.

The pars triangularis is the fan-shaped expansion of sensory rootlets that anastomose with each other and that extend posteriorly from the sinus ganglii (3–6, 9, 23). The motor root of CN V passes inferior to the trigeminal ganglion (9) and is adherent to the basal wall of the Meckel cave in its distal portion (6).

MR Imaging

Most previous studies of the trigeminal ganglion were performed using contrast-enhanced T1-weighted sequences (10, 24–26). For example, Downs et al (10) reported enhancement of the trigeminal ganglion in 100% of such studies. One report addressed the possibility of identifying the trigeminal ganglion with T2-weighted fast spin-echo and nonenhanced 3D CISS sequences (24), but other authors could not replicate the findings (13, 14). To our knowledge, no previous reports have addressed the true dimensions of the ganglion, its extension in the Meckel cave, the sinus ganglii and its lips, or the reliability of displaying the sensory and motor rootlets in the cave.

3D CISS Sequences.—The 3D CISS sequence is a high-spatial-resolution, refocused gradient-echo MR imaging sequence that is flow compensated. It can be performed with thin (0.66-mm) sections, and it can depict small structures surrounded by CSF with high contrast and high spatial resolution. Therefore, the sequence is useful for MR cisternography and has been successfully applied to visualize small cisternal structures, such as the trochlear nerve (18), the abducens nerve (17), and the rootlets of the hypoglossal nerve (17). In all of our patients, the intracisternal portions of the sensory and motor rootlets were well depicted and differentiated from each other with both nonenhanced and contrast-enhanced 3D CISS sequences.

TABLE 4: MR imaging identification of the mandibular, maxillary, and ophthalmic nerves

	V3*			V2†			V1‡		
Study and Plane	2	1	0	2	1	0	2	1	0
Nonenhanced 3D CISS (44 sides)									
Transverse	2 (4.5)	0 (0)	42 (95.5)	0 (0)	0 (0)	44 (100)	0 (0)	1 (2.3)	43 (97.7)
Sagittal	7 (15.9)	11 (25)	24 (54.5)	0 (0)	5 (11.4)	39 (88.6)	0 (0)	18 (18.2)	36 (81.1)
Coronal	6 (13.6)	15 (34.1)	23 (52.3)	0 (0)	0 (0)	22 (100)	0 (0)	0 (0)	44 (100)
Enhanced 3D CISS (44 sides)									
Transverse	26 (59.1)	9 (20.5)	9 (20.5)	18 (41)	22 (50)	4 (9.1)	35 (79.5)	9 (20.5)	0 (0)
Sagittal	44 (100)	0 (0)	0 (0)	24 (54.5)	17 (38.6)	3 (6.8)	39 (88.6)	4 (9.1)	1 (2.3)
Coronal	44 (100)	0 (0)	0 (0)	13 (29.5)	24 (54.5)	7 (15.9)	28 (63.6)	12 (27.3)	4 (9.1)
Enhanced 3D TOF (42 sides)									
Transverse	34 (81)	18 (42.9)	0 (0)	33 (78.6)	8 (19)	0 (0)	39 (92.9)	3 (7.1)	0 (0)
Sagittal	39 (92.9)	3 (7.1)	0 (0)	31 (73.8)	11 (26.2)	0 (0)	38 (90.5)	4 (9.5)	0 (0)
Coronal	42 (100)	0 (0)	0 (0)	30 (71.4)	11 (26.2)	1 (2.4)	30 (71.4)	12 (28.6)	0 (0)

Note.—Data are the numbers of nerves (percentage).

*Inside foramen ovale.

†At the inferior border of the cavernous sinus and inside the foramen rotundum.

‡Inside the lateral wall of the cavernous sinus and the superior orbital fissure.

The trigeminal ganglion, however, lies only partially within the trigeminal cistern. The convex anteroinferior surface of the ganglion is adherent to the dura of the Meckel cave and therefore lies outside the trigeminal cistern (2, 3, 5, 6, 22). For that reason, the 3D CISS sequences were not expected to display the ganglion well. The dura and the ganglion had similar signal intensities on nonenhanced CISS images (Fig 2); therefore, nonenhanced were also not expected to depict the ganglion well. However, Shigematsu et al (27) demonstrated that contrast-enhanced 3D CISS sequences show increased signal intensity that is directly proportional to the concentration of gadopentate dimeglumine administered. Therefore, should the dura and the ganglion enhance to different degrees after the administration of contrast material, contrast-enhanced 3D CISS images should successfully distinguish the trigeminal ganglion from the adjacent dural wall of the Meckel cave and display the ganglion well. This postulate was confirmed. In our study, identification of the trigeminal ganglion (score of 2) improved from 15.9% on nonenhanced 3D CISS images to 79.5% on contrast-enhanced 3D CISS images (Figs 2–4, Table 1). Identification of the ganglion lips improved from 43.2% with the nonenhanced 3D CISS sequence to 95.5% with the enhanced 3D CISS sequence. The thickness of the ganglion were measured on 97.8% of contrast-enhanced 3D CISS images but 59.1% of nonenhanced 3D CISS images (Tables 2 and 3)

T1-Weighted MR Images.—In the series by Downs et al (10), the trigeminal ganglion was identified as an enhancing, semilunar structure in 88% of their coronal T1-weighted spin-echo MR images. In 12%, however, the enhancing ganglion was to be appreciated only as a thickening that blended with the dura. These results are in line with our findings on contrast-enhanced 3D TOF images. Our T1-weighted TOF studies depicted the trigeminal ganglion (scores of 1 or 2) on 80.9% of coronal images, 92.9% of sagittal images (Fig 3), and 78.6% of transverse images. The contrast enhancement of the ganglion blended with that of the dural wall of the Meckel cave on 19% of coronal images, making it difficult to differentiate the two structures and to measure the size of the ganglion (Table 1).

We deliberately used the 3D TOF sequence instead of conventional T1-weighted spin-echo or fast (turbo) spin-echo sequences because the 3D TOF sequence allowed for thin (1-mm) sections for ready reconstruction along the oblique planes needed to follow the course of the nerves and for improved contrast enhancement achieved by saturating the background soft tissue. Nevertheless, the 3D TOF sequence depicted the ganglion lips with certainty in only 9.5% of sides (vs. 95.5% for contrast-enhanced 3D CISS images), and the images failed to depict the sensory and motor rootlets in the trigeminal cistern (Fig 5, Table 3).

Contrast Enhancement of the Trigeminal Ganglion.—Reports about the contrast enhancement of the trigeminal ganglion are discordant. Downs et al (10) reported enhancement of the trigeminal ganglion on all coronal T1-weighted spin-echo MR images. Williams et al (26) found enhancement in 4% of cases and stated that the ganglial enhancement that Downs et al reported might represent enhancement of a pericavernous venous plexus engulfing the ganglion. This pericavernous venous plexus is a well-described feature that Rhoton reported (8). It converges on the cavernous sinus, with the lateral edge of its posterior wall lying just medial to the ostium of the Meckel cave and medial to the upper third of the trigeminal ganglion but not situated in the Meckel cave (8). Furthermore, we found no description of a venous plexus in the Meckel cave or directly surrounding the dural sheath of the ganglion in any previous anatomic report.

The ganglion enhanced more than the adjacent dura in 92.9% of sides on contrast-enhanced 3D TOF imaging, and all sides on contrast-enhanced 3D CISS imaging (Figs 3–5). These findings support the hypothesis that the trigeminal ganglion does enhance

appreciably, as Downs and co-workers originally suggested (10).

Ophthalmic, Maxillary, and Mandibular Nerves

Anatomy.—V1 courses anteriorly in the lateral wall of the cavernous sinus (2, 8, 13). It enters the orbit through the superior orbital fissure (21), a bony hiatus 20 mm long by 6 mm wide that contains an anterior extension of the cavernous sinus (28). The major portion of V2 courses below the line of junction of the medial and lateral walls of the cavernous sinus (8). It exits the skull through the foramen rotundum (21), a narrow canal approximately 4 mm long and 3 mm wide (6). V3 courses inferiorly to exit the skull through the foramen ovale, an ostium 7 mm long by 4 mm wide (5, 21).

MR Imaging of V1, V2, and V3.—Previous MR imaging studies involved a systematic identification of the three major trigeminal branches with nonenhanced and contrast-enhanced T1-weighted sequences (1, 24, 26, 29), nonenhanced T2-weighted fast spin-echo sequences (24), and nonenhanced 3D CISS sequences (24). In studies of contrast enhanced T1-weighted sequences, V2 and V3 were visualized in the foramina ovale and rotundum in up to 93% of cases, but the authors did not report on visualization of V1 (14, 26). To our knowledge, we are first to assess the cranial segments of all three major branches of CN V by using contrast-enhanced 3D CISS and 3D TOF images, which successfully depicted V1, V2, and V3 on 84.1–93.2% and 97.6–100% of the images, respectively (Figs 3–5, Table 4).

The improvement in visualizing the foraminal and cranial segments of V1, V2, and V3 most likely resulted from enhancement of the perineural venous plexus that surrounds each nerve within the foramen. Because the nerves do not enhance, they are displayed as linear structures of low signal intensity within the high signal intensity, enhancing venous plexus (14, 17, 26, 30).

In most cases, contrast-enhanced 3D TOF MR images successfully depicted V1 in the lateral wall of the cavernous sinus and the superior orbital fissure, V2 along the inferior border of the cavernous sinus and in foramen rotundum, and V3 in the foramen ovale (Fig 5). Compared with nonenhanced 3D CISS sequences, the enhanced 3D CISS sequence dramatically improved the identification of V1, V2, and V3 in all three planes (Figs 2–4). Overall, the enhanced T1-weighted 3D TOF sequence was superior to the enhanced 3D CISS sequence and appeared to be the most suitable sequence for depicting the main trigeminal branches (Table 4).

Study Limitations

We did not have a true reference standard. This could have been achieved by imaging the specimens in whom cryomicrotomic sections were later obtained. The role of contrast enhancement, however, could not have been evaluated in that group. Another approach would have been to evaluate patients undergoing surgery for the Meckel cave and to compare the MR images with *in vivo* photographs and surgical descriptions. Because we excluded patients with disease of CN V, this approach was also not possible. We tried to circumvent this problem by comparing our imaging results with the classic anatomic descriptions of this well-studied structure and with the cryomicrotomic sections we obtained. Nevertheless, the absence of a direct criterion standard is a drawback of our study, as in many other anatomic imaging studies (14, 26).

Conclusion

Contrast-enhanced 3D CISS images exquisitely displayed the trigeminal ganglion, the sinus ganglii, and the sinus lips. The motor root of CN V was clearly distinguishable from the sensory rootlets of the pars triangularis in the Meckel cave. Enhanced 3D CISS images also depicted the trigeminal branches V1 (91–100%), V2 (84–93%), and V3 (80–100%) but not as well as enhanced 3D TOF images (97.6–100% for all divisions). Therefore, the contrast-enhanced 3D CISS sequences appeared to be the most appropriate sequence for evaluating the trigeminal ganglion, whereas contrast-enhanced 3D TOF sequences were most appropriate for depicting the cranial and foraminal segments of V1, V2 and V3. Complete MR imaging evaluation of the trigeminal ganglion and roots is best performed using both contrast-enhanced 3D CISS and contrast-enhanced 3D TOF MRA sequences.

References

1. Leblanc A. *Encephalo-Peripheral Nervous System. Vascularisation, Anatomy, Imaging.* 2nd ed. Berlin: Springer-Verlag; 2001:81–210
2. Kehrli P, Maillot C, Wolff M-J **Anatomy and embryology of the trigeminal nerve and its branches in the parasellar area.** *Neurol Res* 1997;19:57–65
3. Chui M, Tucker W, Hudson A, Bayer N. **High resolution CT of Meckel's cave.** *Neuroradiology* 1985;27:403–409
4. Rubinstein D, Stears RLG, Stears JC. **Trigeminal nerve and ganglion in the Meckel cave: appearance at the CT and MR imaging.** *Radiology* 1994;193:155–159
5. Ferner H. **On the anatomy of the intracranial segments of the trigeminal nerve [in German].** *Z Anat Entwicklungsgesch* 1948;114:108–122
6. Lang J. *Clinical Anatomy of the Head: Neurocranium, Orbit, Craniocervical Regions.* Berlin: Springer-Verlag; 1983:186–203
7. Lang J. **Neuroanatomy of the optic, trigeminal, facial, glossopharyngeal, vagus, accessory and hypoglossal nerves [in German].** *Arch Otorhinolaryngol* 1981;231:1–69
8. Rhoton AL. **The cavernous sinus, the cavernous venous plexus, and the carotid collar [Suppl].** *Neurosurgery* 2002;51:375–410
9. Ferner H. **On the structure of the semilunar ganglion (Gasseri) and the trigeminal nerve root in men [in German].** *Z Anat Entwicklungsgesch* 1940;110:391–404
10. Downs DM, Damiano TR, Rubinstein D. **Gasserian ganglion: appearance on contrast-enhanced MR.** *AJNR Am J Neuroradiol* 1996;17:237–241
11. Akimoto H, Nagaoka T, Nariai T, Takada Y, Ohno K, Yoshino N. **Preoperative evaluation of neurovascular compression in patients with trigeminal neuralgia by use of three-dimensional reconstruction from two types of high resolution magnetic resonance imaging.** *Neurosurgery* 2002;51:956–961
12. Yamakami I, Kobayashi E, Hirai S, Yamaura A. **Preoperative assessment of trigeminal neuralgia and hemifacial spasm using constructive interference in steady state-three-dimensional Fourier**

transformation magnetic resonance imaging. *Neurol Med Chir (Tokyo)* 2000;40:545–556
13. Go JL, Kim PE, Zee CS. **The trigeminal nerve.** *Semin Ultrasound CT MRI* 2001;22:502–520
14. Castillo M**. Imaging of the upper cranial nerves I, III-VIII, and the cavernous sinuses.** *Magn Reson Imaging Clin N Am* 2002;10:415–431
15. Rhoton AL. **The cerebellopontine angle and posterior fossa cranial nerves by the retrosigmoid approach.** *Neurosurgery* 2000;47:S93–S129
16. Harris FS, Rhoton AL. **Anatomy of the cavernous sinus. A microsurgical study.** *J Neuosurg* 1976;45:169–180
17. Yousry I, Camelio S, Wiesmann M, et al. **Detailed MR anatomy of the cisternal segment of the abducens nerve: Dorello's canal, neurovascular relationships and landmarks.** *J Neurosurg* 1999;91:276–283
18. Yousry I, Moriggl M, Dieterich M, Naidich TP, Schmid UD, Yousry TA. **MR anatomy of the proximal cisternal segment of the trochlear nerve: neurovascular relationships and landmarks.** *Radiology* 2002;223:31–38
19. Yousry I, Camelio S, Schmid UD, et al. **Visualization of cranial nerves I-XII: value of 3D CISS and T2w-FSE sequences.** *Eur Radiol* 2000;10:1061–1067
20. Yousry I, Moriggl B, Schmid UD, et al. **Detailed anatomy of the intracranial segment of the hypoglossal nerve: neurovascular relationships and landmarks on magnetic resonance imaging sequences.** *J Neuosurg* 2002;96:1113–1122
21. Nemzek WR. **The trigeminal nerve.** *Top Magn Reson Imaging* 1996;8:132–154
22. v. Lanz T, Wachsmuth W. *Praktische Anatomie: Gehirn und Augenschädel.* Vol. 1. Berlin: Springer-Verlag; 1979:78–85
23. Jannetta PJ. **Gross (mesoscopic) description of the human trigeminal nerve and ganglion.** *J Neurosurg* 1967;26:109–111
24. Held P, Fründ R, Seitz J, Nitz W, Haffke T, Hees H. **Comparison of 2-D turbo spin echo and 3-D gradient echo sequences for the detection of the trigeminal nerve and branches anatomy.** *Eur J Radiol* 2001;37:18–25
25. Benoudiba F, Hadj-Rabia M, Iffenecker C, et al. **Variantes anatomiques du cavum de Meckel en IRM.** *J Neuroradiol* 1998;25:201–206
26. Williams LS, Schmalfuss IM, Sistrom CL, et al. **MR Imaging of the trigeminal ganglion, nerve, and the perineural vascular plexus: normal appearance and variants with correlation to cadaver specimens.** *AJNR Am J Neuroradiol* 2003;24:1317–1323
27. Shigematsu Y, Korogi Y, Hirai T, et al. **Contrast-Enhanced CISS MRI of vestibular schwannomas: phantom and clinical studies.** *JCAT* 1999;23:224–231
28. Morard M, Tcherekayev V, de Tribolet N**. The superior orbital fissure: a microanatomical study.** *Neurosurgery* 1994;35:1087–1093
29. Martin-Duverneuil N, Sarrazin JL, Gayet-Delacroix M, Marsot-Dupuch K, Plantet MM. **The foramen rotundum. Anatomy and radiological explorations. Pathology [in French].** *J Neuroradiol* 2000;27:2–14
30. Voyvodic F, Whyte A, Slavotinek J**. The hypoglossal canal: normal MR enhancement pattern**. *AJNR Am J Neuroradiol* 1995;16:1707–1710